



1 **Socio-hydrologic data assimilation: Analyzing human-flood interactions by model-**

2 **data integration**

3

4 Yohei Sawada¹, Risa Hanazaki²

5 ¹ Institute of Engineering Innovation, School of Engineering, the University of Tokyo,

6 Tokyo, Japan

7 ² Institute of Industrial Science, the University of Tokyo, Tokyo, Japan

8

9

10 Corresponding author: Y. Sawada, Institute of Engineering Innovation, the University of

11 Tokyo, Tokyo, Japan, 2-11-6, Yayoi, Bunkyo-ku, Tokyo, Japan, yohei.sawada@sogo.t.u-

12 tokyo.ac.jp

13



14 **Abstract**

15 In socio-hydrology, human-water interactions are simulated by mathematical models.
16 Although the integration of these socio-hydrologic models and observation data is
17 necessary to improve the understanding of the human-water interactions, the
18 methodological development of the model-data integration in socio-hydrology is in its
19 infancy. Here we propose to apply sequential data assimilation, which has been widely
20 used in geoscience, to a socio-hydrological model. We developed particle filtering for a
21 widely adopted flood risk model and performed an idealized observation system
22 simulation experiment to demonstrate the potential of the sequential data assimilation in
23 socio-hydrology. In this experiment, the flood risk model's parameters, the input forcing
24 data, and empirical social data were assumed to be somewhat imperfect. We tested if data
25 assimilation can contribute to accurately reconstructing the historical human-flood
26 interactions by integrating these imperfect models and imperfect and sparsely distributed
27 data. Our results highlight that it is important to sequentially constrain both state variables
28 and parameters when the input forcing is uncertain. Our proposed method can accurately
29 estimate the model's unknown parameters even if the true model parameter temporally
30 varies. The small amount of empirical data can significantly improve the simulation skill



31 of the flood risk model. Therefore, sequential data assimilation is useful to reconstruct

32 historical socio-hydrological processes by the synergistic effect of models and data.

33

34



35

36 **1. Introduction**

37 Socio-hydrology is an emerging research field in which two-way feedbacks between
38 social and water systems are investigated (Sivapalan et al. 2012, 2014). Understanding
39 complex socio-hydrologic phenomena contributes to solving water crises around the
40 world. Socio-hydrology has been recognized as an important scientific grand challenge
41 to meet United Nations' Sustainable Development Goals (Di Baldassarre et al. 2019).

42

43 The most popular approach in socio-hydrology is to develop dynamic models which
44 compute non-linear interactions between human and water. For instance, Di Baldassarre
45 et al. (2013) developed a simplified model, which described human-flood interactions, to
46 understand the levee effect in which high levees generate a false sense of security and
47 induce social vulnerabilities to severe floods (see also Viglione et al. 2014; Ciullo et al.
48 2017). Van Emmerik et al. (2014) developed a stylized model, which described two-way
49 feedbacks between environment and economic activities, to understand the historical
50 competition for water between agricultural development and environment health in
51 Australia (see also Roobavannan et al. 2017). Pande and Savenije (2016) modeled
52 economic activities of smallholder farmers to analyze the agrarian crisis in Marathwada,
53 India. While socio-hydrologic models described above assumed the existence of a single



54 lumped decision maker, Yu et al. (2017) incorporated a collective action into their model
55 and analyzed the dynamics of community-managed flood protection systems in coastal
56 Bangladesh. Please refer to Di Baldassarre et al. (2019) for the comprehensive review of
57 socio-hydrologic modeling.

58

59 In addition to these modeling approaches, both qualitative and quantitative data related to
60 socio-hydrologic processes are important to understand human-water interactions. For
61 instance, Mostert (2018) revealed historical changes in river management from water
62 resources development to protection and restoration by analyzing qualitative data. Dang
63 and Konar (2018) applied econometric methods to analyze quantitative data in both
64 human and water domains and quantified the causal relationship between trade openness
65 and water use. Kreibich et al. (2017) performed the detailed case study analysis on paired
66 floods, consecutive flood events which occurred in the same region with the second flood
67 causing significantly lower damage. They found that the reduction of vulnerability played
68 a key role for successful adaptation to the second floods.

69

70 Although it is expected that the integration of model and data contributes to accurately
71 understanding the socio-hydrologic processes (Mount et al. 2016), the methodological



72 development of the model-data integration in socio-hydrology is in its infancy. Generally,
73 mathematical models can provide spatiotemporally continuous state variables and
74 quantitative scenarios for future socio-hydrologic developments. In addition,
75 mathematical models can quantitatively provide possible scenarios unrealized in the real-
76 world, which gives the insight to targeted processes (e.g., Viglione et al. 2014). The major
77 limitation of socio-hydrological models is that they are often inaccurate due to the
78 uncertainty in their input forcing, parameters, and descriptions of the processes. On the
79 other hand, hydrologic and social data are often more reliable than numerical models and
80 can provide more complete understanding of the socio-hydrological processes (e.g.,
81 Mostert 2018), although data also have uncertainties. However, in many cases, relevant
82 data in socio-hydrology are sparsely distributed so that it is difficult to completely
83 reconstruct the historical socio-hydrologic processes from data. The other limitation of
84 the data-driven approach is that the quantification of the causal relationship cannot be
85 easily done only by empirical data (e.g., Dang and Konar 2018). Considering this
86 advantages and disadvantages of model and data, previous studies used social statistics
87 to calibrate and validate their socio-hydrologic models (e.g., Barendrecht et al. 2019;
88 Roobavannan et al. 2017; Ciullo et al. 2017; van Emmerik et al. 2014; Gonzales and
89 Ajami 2017).



90

91 In geosciences, sequential data assimilation has been widely used for the model-data
92 integration. Data assimilation sequentially adjusts the predicted state variables and
93 parameters of dynamic models by integrating observation data into models based on
94 Bayes' theorem. Data assimilation has been widely applied to numerical weather
95 prediction (e.g., Miyoshi and Yamane 2007; Bauer et al. 2015; Poterjoy et al. 2019;
96 Sawada et al. 2019), atmospheric reanalysis (e.g., Kobayashi et al. 2015; Hersbach et al.
97 2019), and hydrology and land surface modeling (e.g., Moradkhani et al. 2005; Sawada
98 et al. 2015; Rasmussen et al. 2015; Lievens et al. 2017). Applicability of the data
99 assimilation approach to the socio-hydrologic models has yet to be investigated.

100

101 In this study, we aim to develop the methodology of sequential data assimilation for the
102 flood risk model proposed by Di Baldassarre et al. (2013). From a series of idealized
103 experiments, we demonstrate the potential of data assimilation to accurately reconstruct
104 the historical human-flood interactions. We focus on the case in which the socio-
105 hydrologic model's parameters, input forcing data, and social data are somewhat
106 inaccurate.

107



108

109 2. Method

110 2.1. Model

111 In this study, we used a socio-hydrologic flood risk model proposed by Di Baldassarre et
112 al. (2013). This model conceptualizes human-flood interactions by the set of simple
113 equations which describe the states of flood, economy, technology, politics, and society.
114 Based on this original model of Di Baldassarre et al. (2013), many similar flood risk
115 models have been proposed, validated, and applied (e.g., Viglione et al. 2014; Ciullo et
116 al. 2017; Barendrecht et al. 2019). Here we briefly describe this model. Please refer to Di
117 Baldassarre et al. (2013) for the complete description of this model.

118

119 The governing equations of the flood risk model are shown below:

$$120 \quad F = \begin{cases} 1 - \exp\left(-\frac{W + \xi_H H}{\alpha_H D}\right) & \text{if } W + \xi_H H > H \\ 0 & \text{if } W + \xi_H H \leq H \end{cases} \quad (1)$$

$$121 \quad R = \begin{cases} \varepsilon_T (W + \xi_H H - H) & \text{if } (F > 0) \text{ and } (FG > \gamma_E R \sqrt{G}) \text{ and } (G - FG > \gamma_E R \sqrt{G}) \\ 0 & \text{otherwise} \end{cases}$$

122 (2)

$$123 \quad S = \begin{cases} \alpha_S F & \text{if } (R > 0) \\ F & \text{if } (R = 0) \end{cases} \quad (3)$$

$$124 \quad \frac{dG}{dt} = \rho_E \left(1 - \frac{D}{\lambda_E}\right) G - \Delta(Y(t))(FG + \gamma_E R \sqrt{G}) \quad (4)$$



$$125 \quad \frac{dD}{dt} = \left(M - \frac{D}{\lambda_P}\right) \frac{\varphi_P}{\sqrt{G}} \quad (5)$$

$$126 \quad \frac{dH}{dt} = \Delta(Y(t))R - \kappa_T H \quad (6)$$

$$127 \quad \frac{dM}{dt} = \Delta(Y(t))S - \mu_S M \quad (7)$$

128

129 This model has four state variables: G , D , H , and M . $G(t)$ [L^2] is the size of the human
130 settlement; $D(t)$ [L] is the distance of the center of mass of the human settlement from the
131 river; $H(t)$ [L] is the flood protection level (or levee height); $M(t)$ [\cdot] is the social
132 awareness of the flood risk.

133

134 Equation (1) calculates the intensity of flooding events $F(t)$ [\cdot] from the high water level
135 $W(t)$ [L], the height of the levee $H(t)$ [L], and the distance of the human settlement from
136 the river $D(t)$ [L]. Equation (2) calculates $R(t)$ [L], the amount by which the levees are
137 raised responding to the flood event. There are three required conditions under which
138 people decide to raise the levee. First, the flood event occurs. Second, the damage of flood
139 (FG) should be larger than the cost of raising levee. Third, the cost of raising levee should
140 be lower than the wealth remaining after the flooding. Equation (3) shows the magnitude
141 of the psychological shock by the flood event $S(t)$ [\cdot]. If the levee is raised, the
142 psychological shock is assumed to be mitigated. Equation (4) explains the dynamics of



143 $G(t)$, the size of the human settlement or the wealth of the community. Following the
144 notation of Di Baldassarre et al. (2013), $\Delta(Y(t)) = 1$ with integral only when time t
145 passes the time of the flooding event ($F > 0$), otherwise, $\Delta(Y(t)) = 0$. The term $FG +$
146 $\gamma_E R \sqrt{G}$ (total cost of flood damage and construction of levees) appears only if flood
147 occurs. Equation (5) shows the dynamics of the distance of the center of mass of the
148 human settlement from the river $D(t)$. When the social awareness of the flood risk is high,
149 people tend to live far from the river. Equation (6) computes the dynamics of the flood
150 protection level $H(t)$ and equation (7) shows the dynamics of the social awareness of the
151 flood risk $M(t)$. The explanation of parameters can be found in Table 1.

152

153

154 **2.2. Data Assimilation**

155 In this study, we used Sampling Importance Resampling Particle Filtering (SIRPF) as the
156 method of data assimilation. SIRPF has been widely used in hydrologic data assimilation
157 (e.g., Moradkhani et al. 2005; Qin et al. 2009; Sawada et al. 2015). Compared with the
158 other data assimilation algorithms such as ensemble Kalman filter, SIRPF is robust
159 against model nonlinearity and associated non-Gaussian error distribution. The
160 disadvantage of SIRPF is that the infeasible computational resources are required if the



161 numerical model is computationally expensive, which is not the case in the flood risk
162 model.

163

164 The flood risk model can be formulated as a discrete state-space dynamic system:

$$165 \quad \mathbf{x}(t + 1) = f(\mathbf{x}(t), \boldsymbol{\theta}, \mathbf{u}(t)) + \mathbf{q}(t) \quad (8)$$

166 where $\mathbf{x}(t)$ is the state variables (i.e. G, D, H, and M), $\boldsymbol{\theta}$ is the model parameters, $\mathbf{u}(t)$
167 is the external forcing (i.e., the high water level), and $\mathbf{q}(t)$ is the noise process which
168 represents the model error. In data assimilation, it is useful to formulate an observation
169 process as follows:

$$170 \quad \mathbf{y}^f(t) = h(\mathbf{x}(t)) + \mathbf{r}(t) \quad (9)$$

171 where $\mathbf{y}^f(t)$ is the simulated observation, h is the observation operator which maps the
172 model's state variables into the observable variables, and $\mathbf{r}(t)$ is the noise process which
173 represents the observation error.

174

175 The SIRPF is a Monte Carlo approximation of Bayesian update of the state variables and
176 parameters:

$$177 \quad p(\mathbf{x}(t), \boldsymbol{\theta} | \mathbf{y}^o(1:t)) \propto p(\mathbf{y}^o(t) | \mathbf{x}(t), \boldsymbol{\theta}) p(\mathbf{x}(t), \boldsymbol{\theta} | \mathbf{y}^o(1:t-1)) \quad (10)$$



178 where $p(\mathbf{x}(t), \boldsymbol{\theta} | \mathbf{y}^o(1:t))$ is the posterior probability of the state variables $\mathbf{x}(t)$ and
179 parameters $\boldsymbol{\theta}$ given all observations up to time t $\mathbf{y}^o(1:t)$. The prior knowledge,
180 $p(\mathbf{x}(t), \boldsymbol{\theta} | \mathbf{y}^o(1:t-1))$, based on the model integration is updated using the likelihood
181 which includes the new observation at time t $p(\mathbf{y}^o(t) | \mathbf{x}(t), \boldsymbol{\theta})$. In this study, we assumed
182 that our observation error follows Gaussian distribution so that the likelihood can be
183 formulated as follows:

$$184 \quad p(\mathbf{y}^o(t) | \mathbf{x}(t), \boldsymbol{\theta}) \equiv L(\mathbf{y}^o(t), \mathbf{x}(t), \boldsymbol{\theta}) =$$
$$185 \quad \frac{1}{\sqrt{\det(2\pi\mathbf{R})}} \exp \left[-\frac{1}{2} (\mathbf{y}^o(t) - \mathbf{y}^f(t))^T \mathbf{R}^{-1} (\mathbf{y}^o(t) - \mathbf{y}^f(t)) \right] \quad (11)$$

186 where \mathbf{R} is the covariance matrix of the observation error process $\mathbf{r}(t)$. The prior
187 knowledge of the state variables is approximated by the ensemble simulation:

$$188 \quad p(\mathbf{x}(t) | \mathbf{y}^o(1:t-1)) \approx \frac{1}{N} \sum_{i=1}^N \delta \left[\mathbf{x}(t) - f \left(\mathbf{x}^i(t-1), \boldsymbol{\theta}^i, \mathbf{u}^i(t-1) \right) \right] \quad (12)$$

189 where N is the ensemble size, $\mathbf{x}^i, \boldsymbol{\theta}^i, \mathbf{u}^i$ are the realizations of the ensemble member i ,
190 and $\delta[\cdot]$ is the Dirac delta function.

191

192 The posterior probability of the state variables and parameters can be approximated as
193 follows:

$$194 \quad p(\mathbf{x}(t) | \mathbf{y}^o(1:t)) \approx \sum_{i=1}^N w(i) \delta(\mathbf{x}(t) - \mathbf{x}^i(t)) \quad (13)$$

$$195 \quad p(\boldsymbol{\theta} | \mathbf{y}^o(1:t)) \approx \sum_{i=1}^N w(i) \delta(\boldsymbol{\theta} - \boldsymbol{\theta}^i) \quad (14)$$



196 where $w(i)$ is the normalized weight for the realization of the ensemble member i and
197 is calculated using the likelihood (see also equation (11)).

$$198 \quad w(i) = \frac{L(y^o(t), x^i(t), \theta^i)}{\sum_{k=1}^N L(y^o(t), x^k(t), \theta^k)} \quad (15)$$

199

200 The implementation of SIRPF is the following:

- 201 1. Model state variables are updated from time $t-1$ to t using ensemble
202 simulation (equations (8) and (12)).
- 203 2. Simulated observations are calculated for all ensembles (equation (9)).
- 204 3. The likelihood for each ensemble member is calculated (equation (11))
- 205 4. The weights are obtained for all ensembles (equation (15))
- 206 5. We applied a resampling procedure according to the normalized weights.

207 The normalized weights of ensemble i , $w(i)$, can be recognized as the
208 probability that the ensemble i is selected after resampling. Resampled state
209 variables and parameters are defined as \mathbf{x}_{resamp}^i and $\boldsymbol{\theta}_{resamp}^i$, respectively.

- 210 6. Since there are no mechanisms to increase the variance of parameters of
211 ensemble members, Moradkhani et al. (2005) proposed to perturb the
212 ensembles of parameters:

$$213 \quad \boldsymbol{\theta}^i \leftarrow \boldsymbol{\theta}_{resamp}^i + \boldsymbol{\varepsilon}^i \quad (16)$$



214 $\varepsilon^i \sim N(0, \max(\omega, s \times Var^\theta))$ (17)

215 where $N(\cdot)$ is the Gaussian distribution, Var^θ is the variance of θ^i , ω
216 is the fixed hyperparameter (see Table 1 for its variable) which guarantees
217 that the ensembles of parameters do not converge into a single value. s is
218 an adaptively changed factor according to the effective ensemble size, N_{eff} .

219 $s = s_0 \left(1 - \left(\frac{N_{eff}}{N}\right)^2\right)$ (18)

220 $N_{eff} = \frac{1}{\sum_{i=1}^N w(i)}$ (19)

221 where $s_0 = 0.05$. The effective ensemble size is the measure of the
222 diversity of ensembles. If the effective ensemble size becomes small,
223 ensembles should be strongly perturbed in order to maintain the diversity of
224 ensembles. Similar strategy has been used in many SIRPF systems (e.g.,
225 Moradkhani et al. 2005; Poterjoy et al. 2019).

226

227

228 3. Experiment design

229 In this study, we performed three observation system simulation experiments (OSSEs).

230 In the OSSE, we generated the synthetic truth of the state and flux variables by driving

231 the flood risk model with the specified parameters and input. Then, we generated



232 synthetic observations by adding the noise to this synthetic truth. Those synthetic
233 observations were assimilated into the model by SIRPF. The performance of SIRPF was
234 evaluated by comparing the estimated state variables by SIRPF with the synthetic truth.
235 Model parameters used to generate the synthetic truth can be found in Table 1. They are
236 identical to Di Baldassarre et al. (2013). The OSSE has been recognized as an important
237 preliminary step to verify the newly developed data assimilation systems (e.g.,
238 Moradkhani et al. 2005; Vrugt et al. 2013; Penny and Miyoshi 2016; Sawada et al. 2018).

239

240 The high water level for the synthetic truth was generated by the following:

$$241 \quad W = \min(v - 10, 0) \quad (20)$$

242 v follows the Gumbel distribution:

$$243 \quad p(v) = \frac{\exp(-\frac{v-\mu}{\beta})}{\beta} \exp(-\exp(-(v-\mu)\beta)) \quad (21)$$

244 where $\mu = 9, \beta = 2.5$. Although our high water level is not identical to Di Baldassarre
245 et al. (2013), the estimated trajectory of the state variables is similar to Di Baldassarre et
246 al. (2013).

247

248 Synthetic observations were generated by adding the Gaussian white noise to the F, G, D,
249 H, and M (see section 2.1) of the synthetic truth. The mean of the Gaussian white noise



250 was 0. The variance of the Gaussian white noise was 10% of the synthetic true variables.

251 We firstly assumed that all of the F, G, D, H, and M can be observed every 10 years or

252 every 10 model integration steps. Then, we evaluated the sensitivity of the observation

253 network (i.e. the observable variables and the observation intervals) to the SIRPF's

254 performance.

255

256 We used the ensemble mean of root-mean square errors (mRMSE) as an evaluation

257 metrics:

$$258 \quad RMSE^i = \sqrt{\frac{1}{T} \sum_{t=1}^T (x^i(t) - z(t))^2} \quad (22)$$

$$259 \quad mRMSE = \frac{1}{N} \sum_{i=1}^N RMSE^i \quad (23)$$

260 where $RMSE^i$ is root-mean-square-error for i th ensemble, T is the computational period,

261 $x^i(t)$ is the simulated state variables of ensemble i at time t , $z(t)$ is the synthetic truth

262 at time t .

263

264

265

266

267 **3.1. Experiment 1: Perfect model with uncertain high water levels**



268 In the first OSSE, we assumed that the model was perfect, and we knew it. We used the
269 same parameter variables as the synthetic truth run and we did not perform the estimation
270 of parameters. Our SIRPF estimated only state variables. Although the model had no
271 uncertainty, it was assumed that the input data, the timeseries of the high water level, were
272 uncertain. Lognormal multiplicative noise was added to the synthetic true high water level
273 so that different ensemble members have different high water levels in the data
274 assimilation experiment. The two parameters of the lognormal distribution, commonly
275 called μ and σ , were set to 0 and 0.15, respectively.

276

277

278 **3.2. Experiment 2: Unknown model parameters and uncertain high water levels**

279 In the second OSSE, we assumed that some of the synthetic true parameter values were
280 unknown. The unknown parameters in the experiment 2 were the cost of levee raising γ_E ,
281 the rate by which new properties can be built φ_P , the rate of decay of levees κ_T , and
282 memory loss rate μ_S (see Table 1). We selected these unknown parameters one by one
283 from four equations of economy, politics, technology, and social (see section 2.1). The
284 initial parameter variables were assumed to be distributed in the bounded uniform
285 distributions whose ranges were found in Table 1. Our SIRPF sequentially assimilated



286 observations and estimated both state variables and parameters in the experiment 2. The
287 high water level data were uncertain as the experiment 1.

288

289

290 **3.3. Experiment 3: Unknown and time-variant model parameters and uncertain**
291 **high water levels**

292 To further demonstrate the potential of sequential data assimilation in socio-hydrology,
293 we assumed that the description of the model was biased in the experiment 3. Here we
294 assumed that one of the model parameters was temporally varied by the unknown
295 dynamics. Specifically, the memory loss rate, μ_S , was temporally varied in the
296 experiment 3:

$$297 \mu_S(t) = \begin{cases} 0.01 & (t < 250) \\ 0.01 + (t - 250) \times \frac{0.10 - 0.01}{500} & (250 \leq t < 750) \\ 0.10 & (750 \leq t) \end{cases} \quad (24)$$

298 In this problem setting, we misunderstood the memory loss rate as a time-invariant
299 parameter in our socio-hydrological model since the dynamics to control the memory loss
300 rate was unknown. We evaluated if SIRPF could track this time-variant parameter and
301 reveal the bias of the model's description. The cost of levee raising γ_E , the rate by which
302 new properties can be built φ_P , and the rate of decay of levees κ_T were assumed to be



303 time-invariant unknown parameters as they were in the experiment 2. The input forcing
304 data, high water level, were uncertain as described in the experiment 1.

305

306

307 **4. Results**

308 **4.1. Experiment 1: Perfect model with uncertain high water levels**

309 Figure 1 shows the timeseries of the model variables calculated by 5000 ensembles with
310 no data assimilation. Although the ensemble mean of the state variables is close to the
311 synthetic truth, the ensembles have the large spread especially for G. The uncertainty in
312 the input forcing brings the uncertainty in the estimation of the historical socio-hydrologic
313 condition.

314

315 Figure 2 indicates that this uncertainty is mitigated by assimilating the observations of F,
316 G, D, H, and M into the model every 10 years with 5000 ensembles. Table 2 shows that
317 RMSE is reduced for all state variables by data assimilation.

318

319 While we can observe all of F, G, D, H, and M in Figure 2 and Table 2, Figure 3 shows
320 the performance of our SIRPF in which only one of them can be observed. Figure 3



321 reveals that we can accurately propagate the observation information into the model state
322 space. In other words, our SIRPF can positively impact the estimation of not only
323 observed state variables but unobserved state variables. For instance, even if we can
324 observe only G, the simulation of all G, D, H, and M is improved. This finding is
325 promising since all of the state variables cannot be observed in the real-world applications.
326 Figure 3 also shows that observing F is not effective compared with the other variables.
327 This is because F is a flux and F can be observed only when floods occur so that the
328 number of effective observations is small. In addition, H is decoupled from the other state
329 variables. Observing F, D, and M negatively impacts the estimation of H and observing
330 H does not significantly improve the simulation of D and M. This is because the dynamics
331 of H is largely determined by high water levels whose uncertainty is not mitigated by our
332 SIRPF system.

333

334 While we can observe every 10 years in Figure 2 and Table 2, Figure 4 shows the
335 sensitivity of the observation intervals to the performance of our SIRPF. Our SIRPF
336 improves the estimation of the state variables when we can obtain observation once in
337 50-year or 100-year (see also Figure S1 for timeseries of the model's variables), which is
338 promising since we cannot expect the frequent observations in the real-world applications.



339

340 Although we demonstrate the potential of our SIRPF with 5000 ensembles thus far, the
341 improvement of the simulation skill can be found in much smaller ensemble sizes. The
342 performance of our SIRPF with 20 ensembles is similar to that with 5000 ensembles
343 (Figure S2).

344

345

346 **4.2. Experiment 2: Unknown model parameters and uncertain high water levels**

347 Figure 5 reveals that the flood risk model completely loses its skill to estimate the human-
348 flood interactions if there are uncertainties in model parameters and high water levels
349 prescribed in Section 3. In contrast to the experiment 1, the ensemble mean cannot
350 accurately reproduce the synthetic truth.

351

352 Figure 6 indicates that our SIRPF can accurately estimate the model state variables by
353 assimilating the observations of F, G, D, H, and M into the model every 10 years with
354 5000 ensembles. Figure 7 indicates that four unknown parameters can also be accurately
355 estimated. We find that it is relatively difficult to estimate the rate of levee's decay, κ_T ,
356 compared with the other parameters. This is because κ_T strongly affects the dynamics



357 of H and the uncertainty in H is largely determined by the uncertainty in high water levels,
358 which is not directly mitigated by our SIRPF system. Table 3 shows that RMSE is reduced
359 for both state variables and parameters by data assimilation.

360

361 We analyzed the impacts of the individual observation types on the simulation skill as we
362 did in the experiment 1. Figure 8a shows that the effects of the individual observation
363 types are similar to what we found in the experiment 1: (1) our SIRPF can improve the
364 skill to simulate unobservable state variables; (2) observing F is not effective compared
365 with the other observations; (3) H is decoupled from the other state variables. Figure 8b
366 reveals that the parameters can be efficiently estimated by assimilating the observation of
367 the state variables which are tightly related to the targeted parameters. For instance,
368 observing D can greatly improve the rate by which new properties can be built, φ_p , in
369 equation (5) which governs the dynamics of D. However, assimilating a single
370 observation type can contribute to accurately estimating all four parameters in many cases,
371 which is the promising result considering the sparsity of the observation in the real-world
372 applications.

373



374 The good performance of our SIRPF can be found with the longer observation intervals
375 as we found in the experiment 1. Figure 9 indicates that our SIRPF can improve the
376 estimation of the state variables and parameters when we can obtain observation once in
377 50-year or 100-year (see also Figures S3 and S4 for timeseries of the model's variables).

378

379 In contrast to the experiment 1, the larger ensemble size is required to stably estimate both
380 state variables and parameters (Figure S5). The increased degree of freedom and the
381 nonlinear relationship between parameters and observations increase the necessary
382 ensemble size.

383

384

385 **4.3. Experiment 3: Unknown and time-variant model parameters and uncertain**

386 **high water levels**

387 In addition to the experiment 2, one of the unknown parameters (μ_S) temporally varies in
388 the synthetic truth of the experiment 3. Figure 10 and Table 4 indicate that despite the
389 error in the model's description, our SIRPF can greatly improve the simulation of the
390 flood risk model. Please note that the synthetic truth shown in Figure 10 is different from
391 that of the previous experiments especially for D and M. Figure 11d indicates that we can



392 accurately estimate the time-variant parameter (μ_S) as well as the other time-invariant
393 parameters (Figures 11a, 11b, and 11c). This result is promising since we cannot expect
394 the perfect description of the socio-hydrologic model in the real-world applications. We
395 also performed the sensitivity test on observation types, observation intervals, and
396 ensemble sizes, which results in the same conclusions as the experiment 2 (not shown).

397

398

399 **5. Discussion**

400 In this study, we developed the sequential data assimilation system for the widely adopted
401 socio-hydrological model, the flood risk model by Di Baldassarre et al. (2013). We
402 demonstrated that our SIRPF for the flood risk model is useful to reconstruct the historical
403 human-flood interactions, which can be called “socio-hydrologic reanalysis”, by
404 integrating sparsely distributed observations and imperfect numerical simulation.
405 Although our experiment design was idealized, this study reveals several important
406 findings toward real-world applications.

407

408 First, the sequential data assimilation can mitigate the negative impact of the uncertainty
409 in the input forcing on the simulation of socio-hydrologic state variables. We found that



410 the small perturbation of high water levels greatly affects the long-term trajectory of the
411 socio-hydrologic state variables as Viglione et al. (2014) found. It is necessary to
412 sequentially constrain the state variables and parameters by sequential data assimilation
413 if the input forcing is uncertain although previous studies on the model-data integration
414 in socio-hydrology mainly focused on parameter calibration assuming no uncertainty in
415 the input forcing (e.g., Barendrecht et al. 2019; Roobavannan et al. 2017; Ciullo et al.
416 2017; van Emmerik et al. 2014; Gonzales and Ajami 2017). To deeply understand the
417 socio-hydrologic processes, the long-term historical analysis should be performed.
418 Although there are many studies on the accurate reconstruction of the historical weather
419 condition (e.g., Toride et al. 2017), it may be necessary to tackle with the uncertainty in
420 hydrometeorological datasets used for the input forcing of the socio-hydrologic models.
421
422 Second, our SIRPF can efficiently improve the simulation of the socio-hydrologic state
423 variables using the sparsely distributed data. All model variables should not necessarily
424 be observed to constrain the model's state variables and parameters. In some cases,
425 observations of a single state variable are enough to reconstruct the accurate socio-
426 hydrologic state. In addition, observation intervals can be longer than 10-year. Since it is
427 difficult to obtain the large volume of data in socio-hydrology, this finding is promising



428 toward real-world applications. We also give some insights about the informative
429 observation types in the flood risk model. With uncertain high water levels, observations
430 of the intensity of flooding events F and the height of levee H are not informative (i.e. the
431 assimilation of these observations cannot greatly improve the simulation skill) although
432 the empirical data which can be related to F and H may be easily found. On the other
433 hand, observations of the size of the human settlement G are informative to constrain the
434 flood risk model. Model parameters can be efficiently estimated by assimilating the state
435 variables which is tightly related to the targeted parameters, which is consistent to the
436 findings of the idealized experiment by Barendrecht et al. (2019).

437

438 Third, our SIRPF is robust to the imperfectness of the socio-hydrologic model. The
439 unknown parameters can be efficiently estimated by the sequential data assimilation.
440 While previous studies evaluated the trajectory in the whole study period to calibrate the
441 socio-hydrologic models by iteratively performing the long-term model integration (e.g.,
442 Barendrecht et al. 2019; Roobavannan et al. 2017; Ciullo et al. 2017; van Emmerik et al.
443 2014; Gonzales and Ajami 2017), we sequentially optimize parameters based on the
444 relatively short-term timeseries allowing parameters to temporally vary in the study
445 period. The advantage of this strategy is that we can deal with time-variant parameters as



446 previously demonstrated in the applications to hydrologic models (e.g., Pathiraja et al.
447 2018). In the model development, parameters are formulated as time-invariant values so
448 that the existence of time-variant parameters indicates the imperfect description of
449 dynamic models. Sequential data assimilation can mitigate the negative impact of this
450 imperfect model description. Vrugt et al. (2013) pointed out that the parameter
451 optimization by the sequential filters is unstable if parameter sensitivity temporally
452 changes (e.g., parameters affects the model's dynamics differently in the different
453 seasons), which may be the potential limitation of our strategy compared with Bayesian
454 inference based on the long-term trajectory such as Barendrecht et al. (2019).

455

456

457 **6. Conclusion**

458 In this study, we proposed to apply the sequential data assimilation to the socio-
459 hydrologic models. By several OSSEs in the flood risk modeling, we found that our
460 proposed SIRPF is robust to the imperfect input forcing and the imperfect model. The
461 sequential data assimilation is useful to reconstruct the socio-hydrologic conditions from
462 the inaccurate and sparsely distributed data and the imperfect simulation. Future work
463 will focus on the verification of our approach by the real data.



464

465

466 **Acknowledgements**

467 We thank Di Baldassarre for sharing the original source code of the flood risk model.

468 Data Integration and Analysis System (DIAS) provided us the computational resources.

469

470 **References**

471 Barendrecht, M. H., Viglione, A., Kreibich, H., Merz, B., Vorogushyn, S., and Blöschl,

472 G.: The Value of Empirical Data for Estimating the Parameters of a

473 Sociohydrological Flood Risk Model. *Water Resources Research*.

474 <https://doi.org/10.1029/2018WR024128>, 2019

475 Bauer, P., Thorpe, A., and Brunet, G.: The quiet revolution of numerical weather

476 prediction. *Nature*, 525(7567), 47–55. <https://doi.org/10.1038/nature14956>, 2015

477 Ciullo, A., Viglione, A., Castellarin, A., Crisci, M., and Di Baldassarre, G.: Socio-

478 hydrological modelling of flood-risk dynamics: comparing the resilience of green

479 and technological systems. *Hydrological Sciences Journal*, 62(6), 880–891.

480 <https://doi.org/10.1080/02626667.2016.1273527>, 2017



- 481 Dang, Q., and Konar, M.: Trade Openness and Domestic Water Use. *Water Resources*
482 *Research*, 54(1), 4–18. <https://doi.org/10.1002/2017WR021102>, 2018
- 483 Di Baldassarre, G., Viglione, A., Carr, G., Kuil, L., Salinas, J. L., and Blöschl, G.: Socio-
484 hydrology: Conceptualising human-flood interactions. *Hydrology and Earth*
485 *System Sciences*, 17(8), 3295–3303. <https://doi.org/10.5194/hess-17-3295-2013>,
486 2013
- 487 Di Baldassarre, G., et al.: Socio-hydrology: Scientific Challenges in Addressing a Societal
488 Grand Challenge. *Water Resources Research*, 1–29.
489 <https://doi.org/10.1029/2018wr023901>, 2019
- 490 Gonzales, P., and Ajami, N.: Social and Structural Patterns of Drought-Related Water
491 Conservation and Rebound. *Water Resources Research*, 53(12), 10619–10634.
492 <https://doi.org/10.1002/2017WR021852>, 2017
- 493 Hersbach, H. et al.: Global reanalysis: goodbye ERA-Interim, hello ERA5, *ECMWF*
494 *Newsletter*, 159, 17-24, doi: [10.21957/vf291hehd7](https://doi.org/10.21957/vf291hehd7), 2019
- 495 Kobayashi, S., et al.: The JRA-55 Reanalysis: General Specifications and Basic
496 Characteristics. *Journal of the Meteorological Society of Japan*, 93, 5-48.
497 <https://doi.org/10.2151/jmsj.2015-001>, 2015



- 498 Kreibich, H., et al.: Adaptation to flood risk: Results of international paired flood event
499 studies. *Earth's Future*. <https://doi.org/10.1002/ef2.232>, 2017
- 500 Lievens, H., et al.: Joint Sentinel-1 and SMAP data assimilation to improve soil moisture
501 estimates. *Geophysical Research Letters*, 44(12), 6145–6153.
502 <https://doi.org/10.1002/2017GL073904>, 2017
- 503 Miyoshi, T., and Yamane, S.: Local Ensemble Transform Kalman Filtering with an
504 AGCM at a T159/L48 Resolution. *Monthly Weather Review*, 135(2002), 3841–
505 3861. <https://doi.org/10.1175/2007MWR1873.1>, 2007
- 506 Moradkhani, H., Hsu, K. L., Gupta, H., and Sorooshian, S.: Uncertainty assessment of
507 hydrologic model states and parameters: Sequential data assimilation using the
508 particle filter. *Water Resources Research*, 41(5), 1–17.
509 <https://doi.org/10.1029/2004WR003604>, 2005
- 510 Mostert, E.: An alternative approach for socio-hydrology: Case study research. *Hydrology
511 and Earth System Sciences*, 22(1), 317–329. [https://doi.org/10.5194/hess-22-317-
512 2018](https://doi.org/10.5194/hess-22-317-2018), 2018
- 513 Mount, N., J., et al.: Data-driven modelling approaches for sociohydrology: opportunities
514 and challenges within the Panta Rhei Science Plan. *Hydrological Sciences Journal*,
515 61(7), 1192-1208. <https://doi.org/10.1080/02626667.2016.1159683>, 2016



- 516 Pande, S., and Savenije, H. H. G.: A sociohydrological model for smallholder farmers in
517 Maharashtra, India. *Water Resources Research*, 52(3), 1923–1947.
518 <https://doi.org/10.1002/2015WR017841>, 2016
- 519 Pathiraja, S., Anghileri, D., Burlando, P., Sharma, A., Marshall, L., and Moradkhani, H.:
520 Time-varying parameter models for catchments with land use change: the
521 importance of model structure, *Hydrol. Earth Syst. Sci.*, 22, 2903–2919,
522 <https://doi.org/10.5194/hess-22-2903-2018>, 2018.
- 523 Penny, S. G., and Miyoshi, T.: *A local particle filter for high-dimensional geophysical*
524 *systems*. 391–405. <https://doi.org/10.5194/npg-23-391-2016>, 2016
- 525 Poterjoy, J., Wicker, L., and Buehner, M.: Progress toward the application of a localized
526 particle filter for numerical weather prediction. *Monthly Weather Review*, 147(4),
527 1107–1126. <https://doi.org/10.1175/MWR-D-17-0344.1>, 2019
- 528 Qin, J., Liang, S., Yang, K., Kaihotsu, I., Liu, R., and Koike, T.: Simultaneous estimation
529 of both soil moisture and model parameters using particle filtering method through
530 the assimilation of microwave signal. *Journal of Geophysical Research*, 114(D15),
531 1–13. <https://doi.org/10.1029/2008JD011358>, 2009
- 532 Rasmussen, J., Madsen, H., Jensen, K. H., and Refsgaard, J. C.: Data assimilation in
533 integrated hydrological modeling using ensemble Kalman filtering: evaluating the



- 534 effect of ensemble size and localization on filter performance. *Hydrology and Earth*
535 *System Sciences*, 19(7), 2999–3013. <https://doi.org/10.5194/hess-19-2999-2015>,
536 2015
- 537 Roobavannan, M., Kandasamy, J., Pande, S., Vigneswaran, S., and Sivapalan, M.: Role
538 of Sectoral Transformation in the Evolution of Water Management Norms in
539 Agricultural Catchments: A Sociohydrologic Modeling Analysis. *Water Resources*
540 *Research*, 53(10), 8344–8365. <https://doi.org/10.1002/2017WR020671>, 2017
- 541 Sawada, Y., Koike, T., and Walker, J. P.: A land data assimilation system for simultaneous
542 simulation of soil moisture and vegetation dynamics. *J. Geophys. Res. Atmos.*, 120,
543 5910– 5930. doi: [10.1002/2014JD022895](https://doi.org/10.1002/2014JD022895), 2015
- 544 Sawada, Y., Nakaegawa, T. and Miyoshi, T.: Hydrometeorology as an inversion problem:
545 Can river discharge observations improve the atmosphere by ensemble data
546 assimilation? *Journal of Geophysical Research: Atmospheres*, 123, 848– 860.
547 <https://doi.org/10.1002/2017JD027531>, 2018
- 548 Sawada, Y., Okamoto, K., Kunii, M., and Miyoshi, T.: Assimilating every-10-minute
549 Himawari-8 infrared radiances to improve convective predictability. *Journal of*
550 *Geophysical Research: Atmospheres*, 124, 2546–2561.
551 <https://doi.org/10.1029/2018JD029643>, 2019



- 552 Sivapalan, M., Savenije, H.H.G. and Blöschl, G.: Socio-hydrology: A new science of
553 people and water. *Hydrol. Process.*, 26: 1270-1276. doi:[10.1002/hyp.8426](https://doi.org/10.1002/hyp.8426), 2012
- 554 Sivapalan, M., Konar, M., Srinivasan, V., Chhatre, A., Wutich, A., Scott, C. A., and
555 Wescoat, J. L.: Socio-hydrology: Use-inspired water sustainability science for the
556 Anthropocene, *Earth's Future*, 2, 225–230. <https://doi.org/10.1002/2013EF000164>,
557 2014.
- 558 Toride, K., Neluwala, P., Kim, H. and Yoshimura, K.: Feasibility Study of the
559 Reconstruction of Historical Weather with Data Assimilation. *Mon. Wea. Rev.*, **145**,
560 3563–3580, <https://doi.org/10.1175/MWR-D-16-0288.1>, 2017
- 561 Van Emmerik, T. H. M., et al.: Socio-hydrologic modeling to understand and mediate the
562 competition for water between agriculture development and environmental health:
563 Murrumbidgee River basin, Australia. *Hydrology and Earth System Sciences*,
564 18(10), 4239–4259. <https://doi.org/10.5194/hess-18-4239-2014>, 2014
- 565 Viglione, A., et al.: Insights from socio-hydrology modelling on dealing with flood risk -
566 Roles of collective memory, risk-taking attitude and trust. *Journal of Hydrology*,
567 518(PA), 71–82. <https://doi.org/10.1016/j.jhydrol.2014.01.018>, 2014
- 568 Vrugt, J. A., ter Braak, C. J. F., Diks, C. G. H., and Schoups, G.: Hydrologic data
569 assimilation using particle Markov chain Monte Carlo simulation: Theory, concepts



570 and applications. *Advances in Water Resources*, 51, 457–478.

571 <https://doi.org/10.1016/j.advwatres.2012.04.002>, 2013

572 Yu, D. J., Sangwan, N., Sung, K., Chen, X., and Merwade, V.: Incorporating institutions

573 and collective action into a sociohydrological model of flood resilience. *Water*

574 *Resources Research*, 53(2), 1336–1353. <https://doi.org/10.1002/2016WR019746>,

575 2017

576

577

578



579

580 **Table 1.** Parameters of the flood risk model

581

	description	Values	Ranges in data assimilation	ω in equation (17)
ξ_H	proportion of additional high water level due to levee heightening	0.5	-	-
α_H	parameter related to the slope of the floodplain and the resilience of the human settlement	0.01	-	-
ρ_E	maximum relative growth rate	0.02	-	-
λ_E	critical distance from the river beyond which the settlement can no longer grow	5000	-	-
γ_E	Cost of levee raising	0.5	0.2-5.0	0.01
λ_P	distance at which people would accept to live when they remember past floods whose total consequences were perceived as a total destruction of the settlement	12000	-	
φ_P	rate by which new properties can be built	10000	1000-50000	100
ε_T	safety factor for levees rising	1.1	-	-
κ_T	rate of decay of levees	0.001	0-0.0015	0.0000025
α_S	proportion of shock after flooding if levees are risen	0.5	-	-
μ_S	memory loss rate	0.05	0-0.4	0.0025

582

583



584 **Table 2.** RMSE of the no data assimilation experiment (NoDA) and the data
585 assimilation experiment (DA) in which all observations are assimilated every 10 years
586 with 5000 ensembles in the experiment 1 (see section 3.1).
587

	NoDA	DA
G	1.06×10^6	1.64×10^4
D	3.60×10^2	3.92×10^1
H	2.65	1.41
M	1.08×10^{-1}	8.32×10^{-2}

588

589



590 **Table 3.** RMSE of the no data assimilation experiment (NoDA) and the data
591 assimilation experiment (DA) in which all observations are assimilated every 10 years
592 with 5000 ensembles in the experiment 2 (see section 3.2).
593

	NoDA	DA
G	2.97×10^6	1.64×10^4
D	1.86×10^3	1.01×10^2
H	9.35	1.63
M	2.24×10^{-1}	8.99×10^{-2}
γ_E	2.08	4.27×10^{-1}
φ_P	1.72×10^4	3.81×10^3
κ_T	4.12×10^{-4}	2.36×10^{-4}
μ_S	1.55×10^{-1}	2.43×10^{-2}

594
595

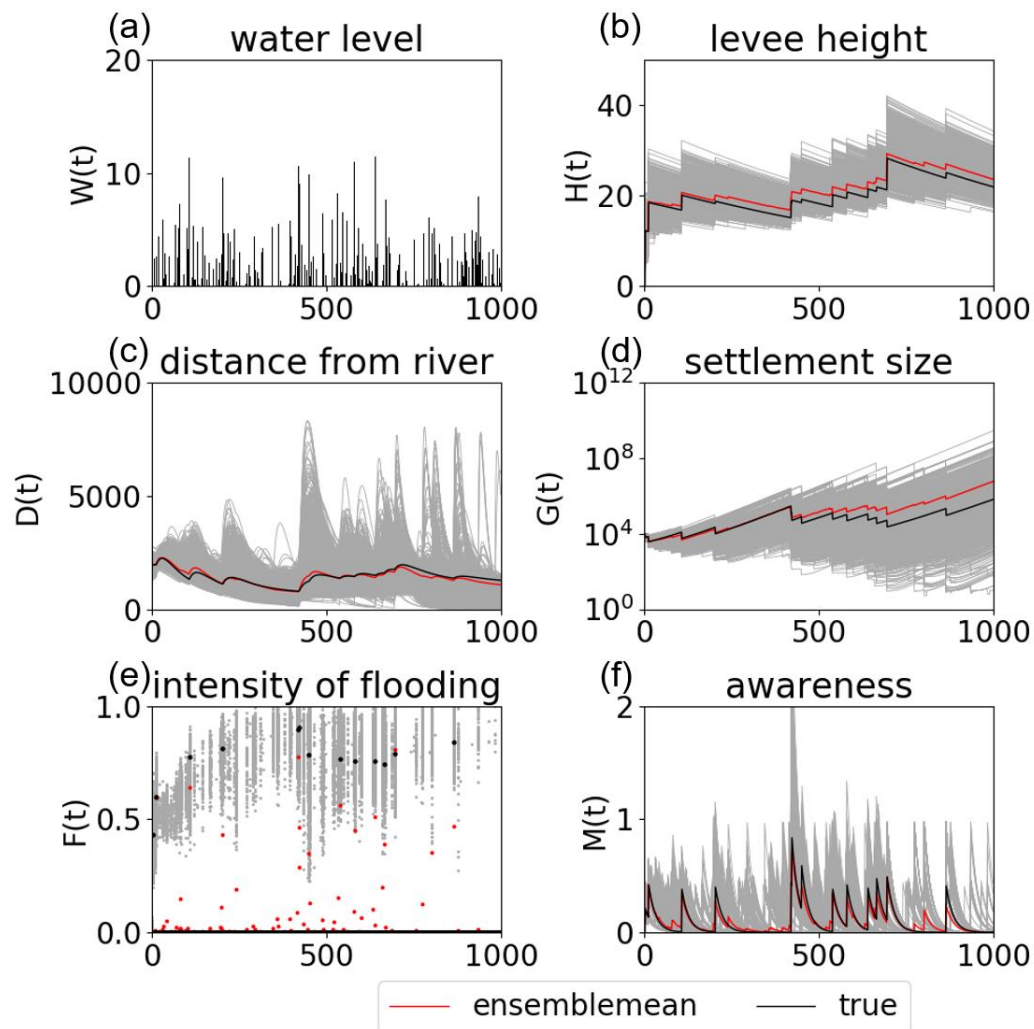


596 **Table 4.** RMSE of the no data assimilation experiment (NoDA) and the data
597 assimilation experiment (DA) in which all observations are assimilated every 10 years
598 with 5000 ensembles in the experiment 3 (see section 3.3).
599

	NoDA	DA
G	2.90×10^6	3.78×10^3
D	2.12×10^3	1.45×10^2
H	9.33	1.62
M	2.45×10^{-1}	7.70×10^{-2}
γ_E	2.08	4.51×10^{-1}
φ_P	1.72×10^4	5.00×10^3
κ_T	4.12×10^{-4}	2.77×10^{-4}
μ_S	1.60×10^{-1}	3.22×10^{-2}

600

601



602

603 **Figure 1.** Timeseries of (a) high water level $W(t)$, (b) the flood protection level (or levee height) $H(t)$, (c) the

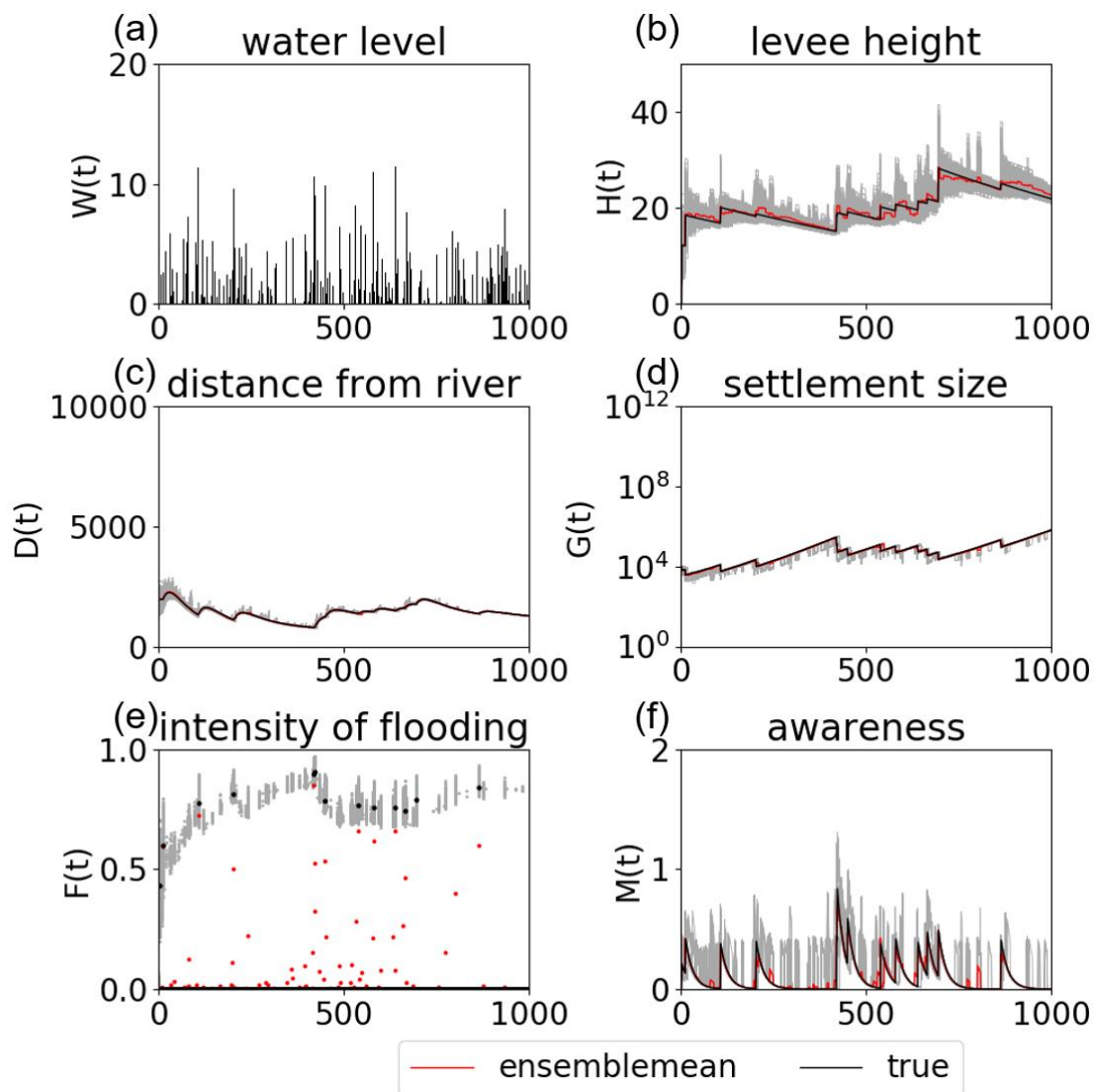
604 distance of the center of mass of the human settlement from the river $D(t)$, (d) the size of the human settlement

605 $G(t)$, (e) the intensity of flooding events $F(t)$, and (f) the social awareness of the flood risk $M(t)$ simulated by

606 5000 ensembles with uncertain high water levels and no data assimilation in the experiment 1 (see section

607 3.1). Grey, red, and black lines are the ensemble members, their mean, and the synthetic truth, respectively.

608

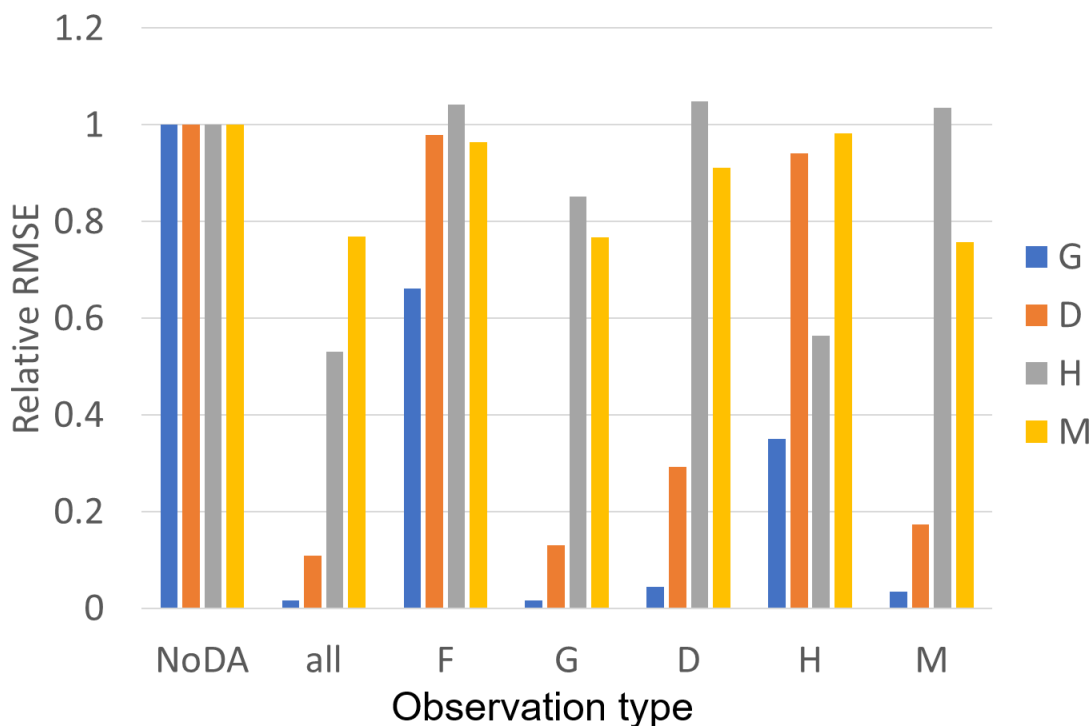


609

610 **Figure 2.** Timeseries of (a) high water level $W(t)$, (b) the flood protection level (or levee height) $H(t)$, (c) the
611 distance of the center of mass of the human settlement from the river $D(t)$, (d) the size of the human settlement
612 $G(t)$, (e) the intensity of flooding events $F(t)$, and (f) the social awareness of the flood risk $M(t)$ simulated by
613 the data assimilation experiment in which the observations of F , G , D , H , and M are assimilated into the model



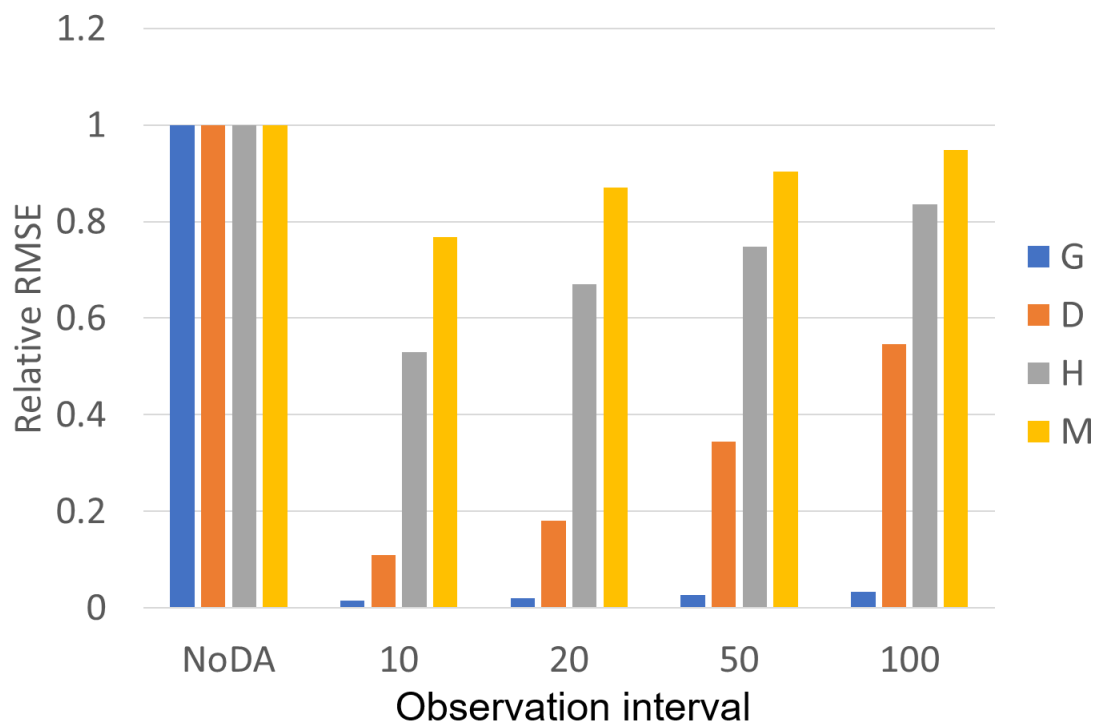
614 every 10 years with 5000 ensembles in the experiment 1 (see section 3.1). Grey, red, and black lines are the
615 ensemble members, their mean, and the synthetic truth, respectively.
616



617

618 **Figure 3.** The ratio of RMSEs of the no data assimilation experiment (NoDA) to those of the data assimilation
619 experiments in which all of observations (F, G, D, H, and M) are assimilated (all) and each one of them is
620 assimilated in the experiment 1 (see section 3.1). Blue, orange, gray, and yellow bars are RMSEs of the size
621 of the human settlement $G(t)$, the center of mass of the human settlement from the river $D(t)$, the flood
622 protection level (or levee height) $H(t)$, and the social awareness of the flood risk $M(t)$.

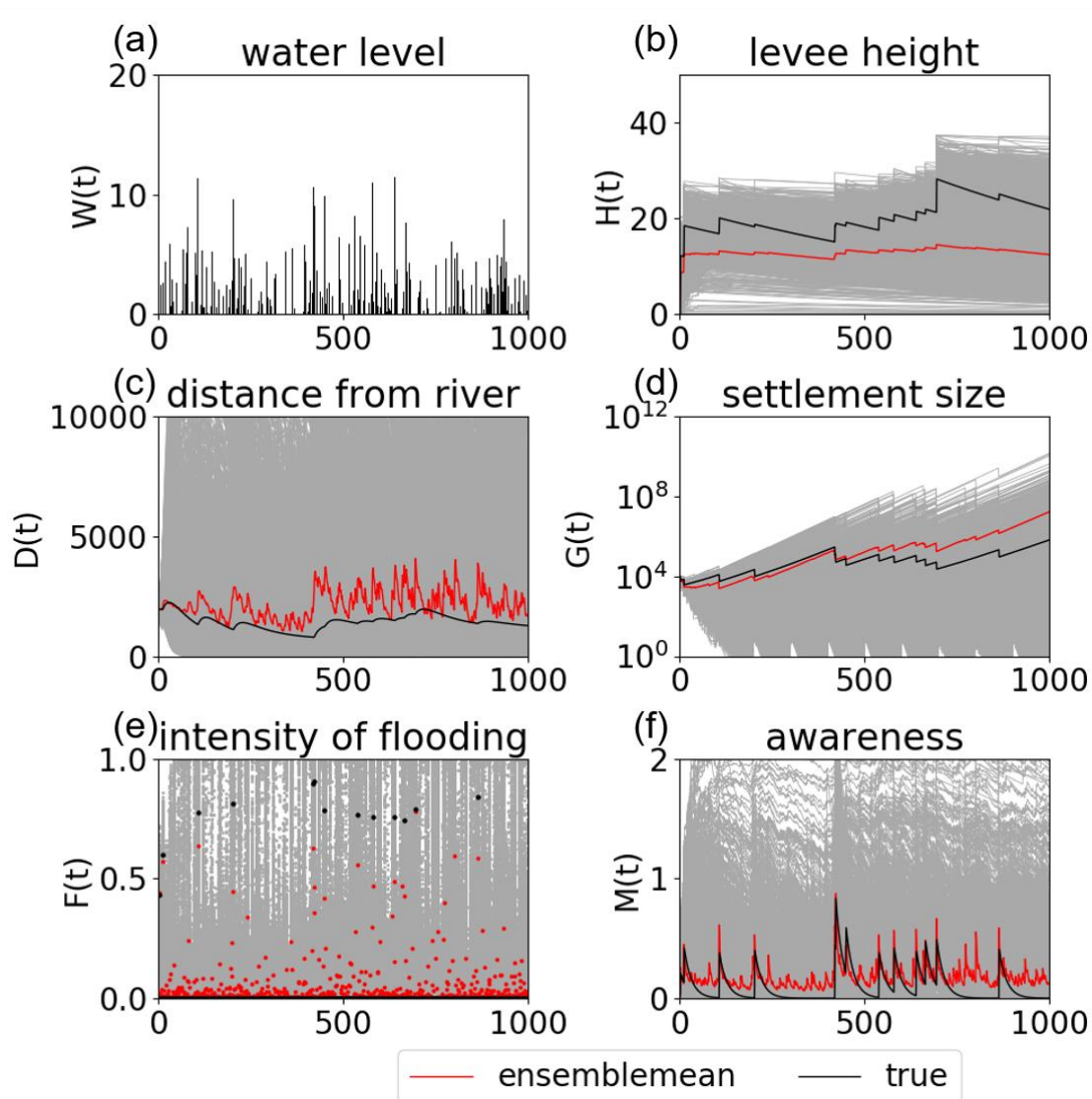
623



624

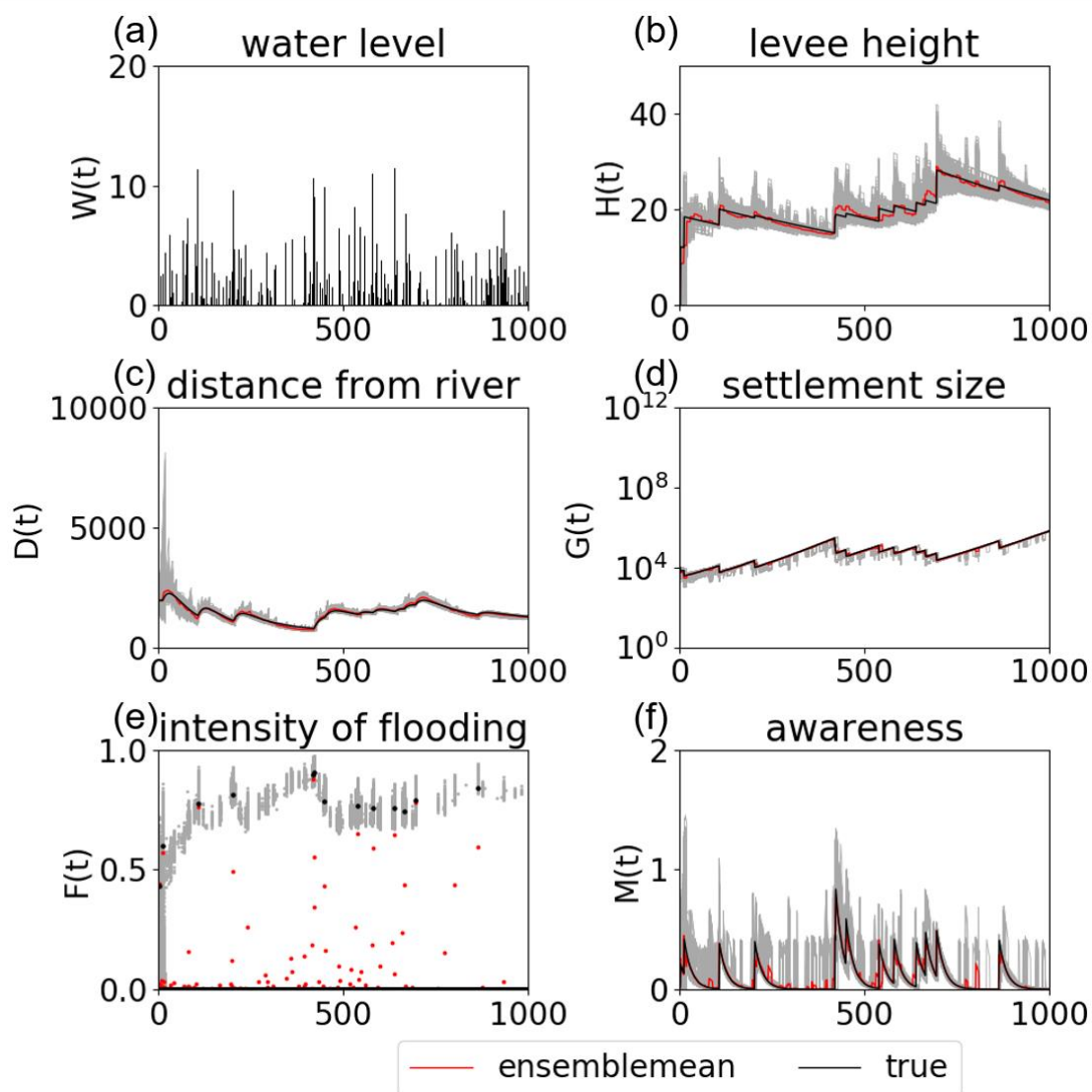
625 **Figure 4.** The ratio of RMSEs of the no data assimilation experiment (NoDA) to those of the data assimilation
626 experiments in which all of observations (F, G, D, H, and M) are assimilated every 10, 20, 50, and 100 years
627 in the experiment 1 (see section 3.1). Blue, orange, gray, and yellow bars are RMSEs of the size of the human
628 settlement $G(t)$, the center of mass of the human settlement from the river $D(t)$, the flood protection level (or
629 levee height) $H(t)$, and the social awareness of the flood risk $M(t)$.

630



631

632 **Figure 5.** Timeseries of (a) high water level $W(t)$, (b) the flood protection level (or levee height) $H(t)$, (c) the
633 distance of the center of mass of the human settlement from the river $D(t)$, (d) the size of the human settlement
634 $G(t)$, (e) the intensity of flooding events $F(t)$, and (f) the social awareness of the flood risk $M(t)$ simulated by
635 5000 ensembles with uncertain high water levels and no data assimilation in the experiment 2 (see section
636 3.2). Grey, red, and black lines are the ensemble members, their mean, and the synthetic truth, respectively.

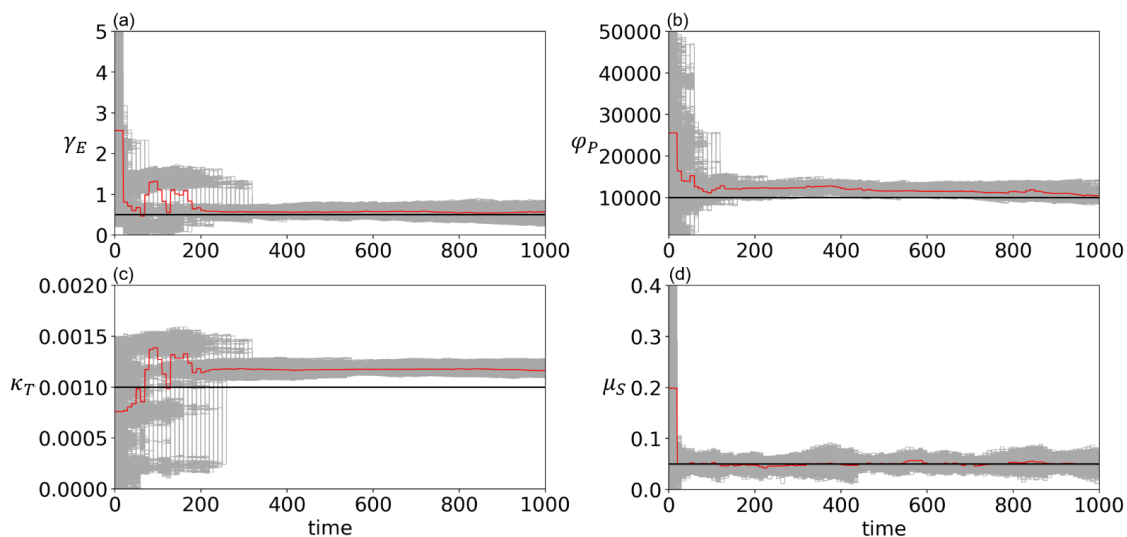


637

638 **Figure 6.** Timeseries of (a) high water level $W(t)$, (b) the flood protection level (or levee height) $H(t)$, (c) the
639 distance of the center of mass of the human settlement from the river $D(t)$, (d) the size of the human settlement
640 $G(t)$, (e) the intensity of flooding events $F(t)$, and (f) the social awareness of the flood risk $M(t)$ simulated by
641 the data assimilation experiment in which the observations of F , G , D , H , and M are assimilated into the model



642 every 10 years with 5000 ensembles in the experiment 2 (see section 3.2). Grey, red, and black lines are the
643 ensemble members, their mean, and the synthetic truth, respectively.



644

645 **Figure 7.** Timeseries of (a) the cost of levee raising γ_E , (b) the rate by which new properties can be built φ_P ,

646 (c) the rate of decay of levees κ_T , (d) memory loss rate μ_S estimated by the data assimilation of all

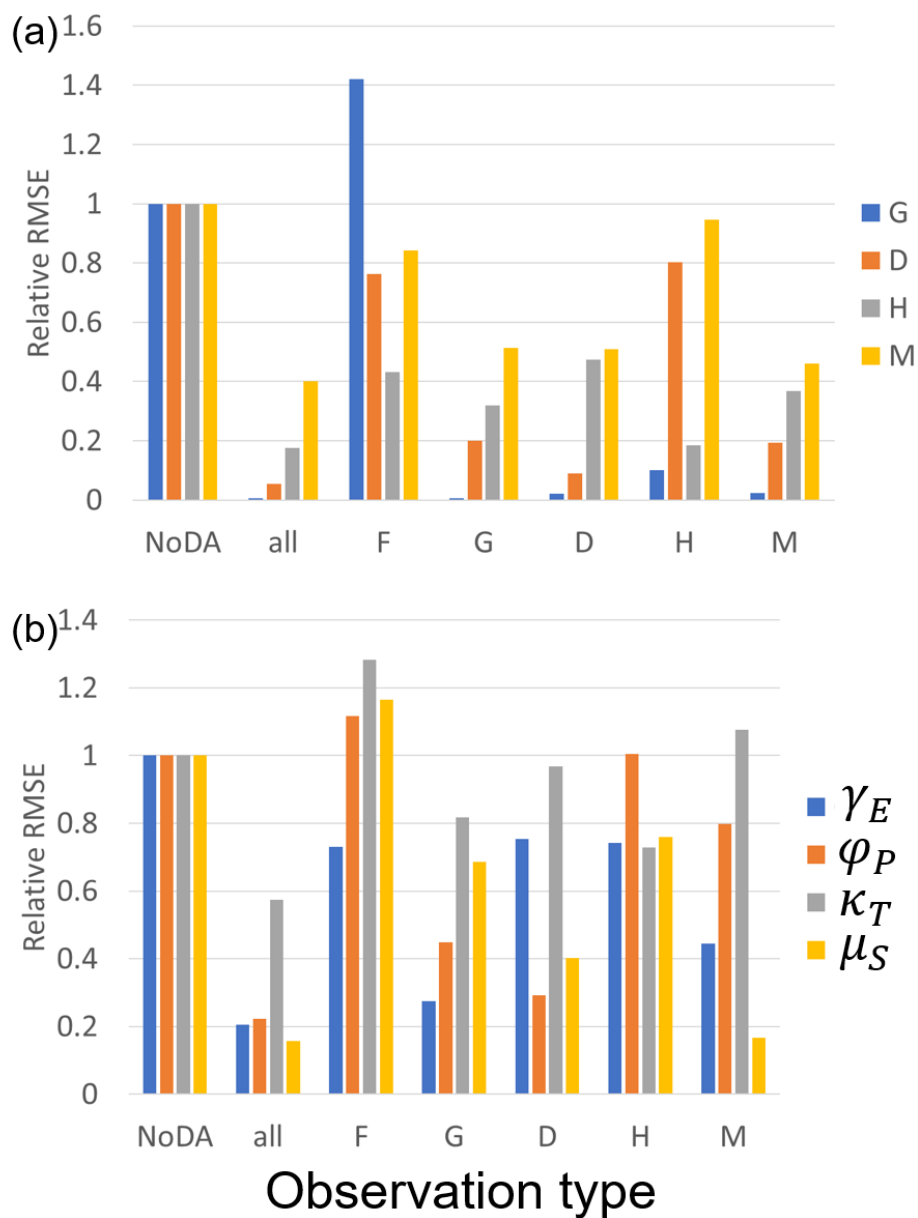
647 observations (F, G, D, H, and M) with 5000 ensembles every 10 years in the experiment 2 (see section 3.2).

648 Grey, red, and black lines are the ensemble members, their mean, and the synthetic truth, respectively.

649



650



651

652 **Figure 8.** The ratio of RMSEs of the no data assimilation experiment (NoDA) to those of the data assimilation

653 experiments in which all of observations (F, G, D, H, and M) are assimilated (all) and each one of them is

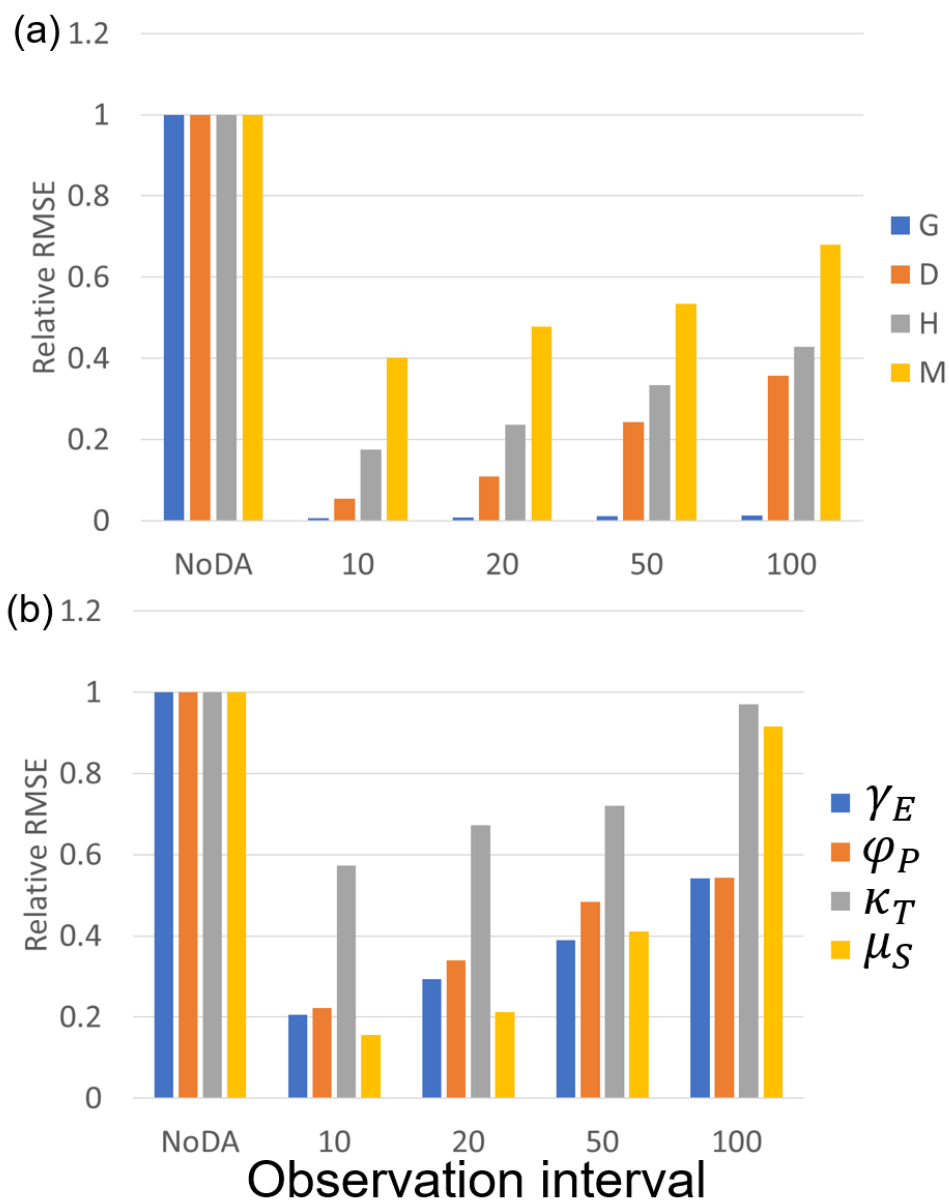
654 assimilated in the experiment 2 (see section 3.2). (a) Blue, orange, gray, and yellow bars are RMSEs of the



655 size of the human settlement $G(t)$, the center of mass of the human settlement from the river $D(t)$, the flood
656 protection level (or levee height) $H(t)$, and the social awareness of the flood risk $M(t)$. (b) Blue, orange, gray,
657 and yellow bars are RMSEs of the cost of levee raising γ_E , the rate by which new properties can be built φ_P ,
658 the rate of decay of levees κ_T , memory loss rate μ_S .

659

660



661

662 **Figure 9.** The ratio of RMSEs of the no data assimilation experiment (NoDA) to those of the data assimilation

663 experiments in which all of observations (F, G, D, H, and M) are assimilated every 10, 20, 50, and 100 years

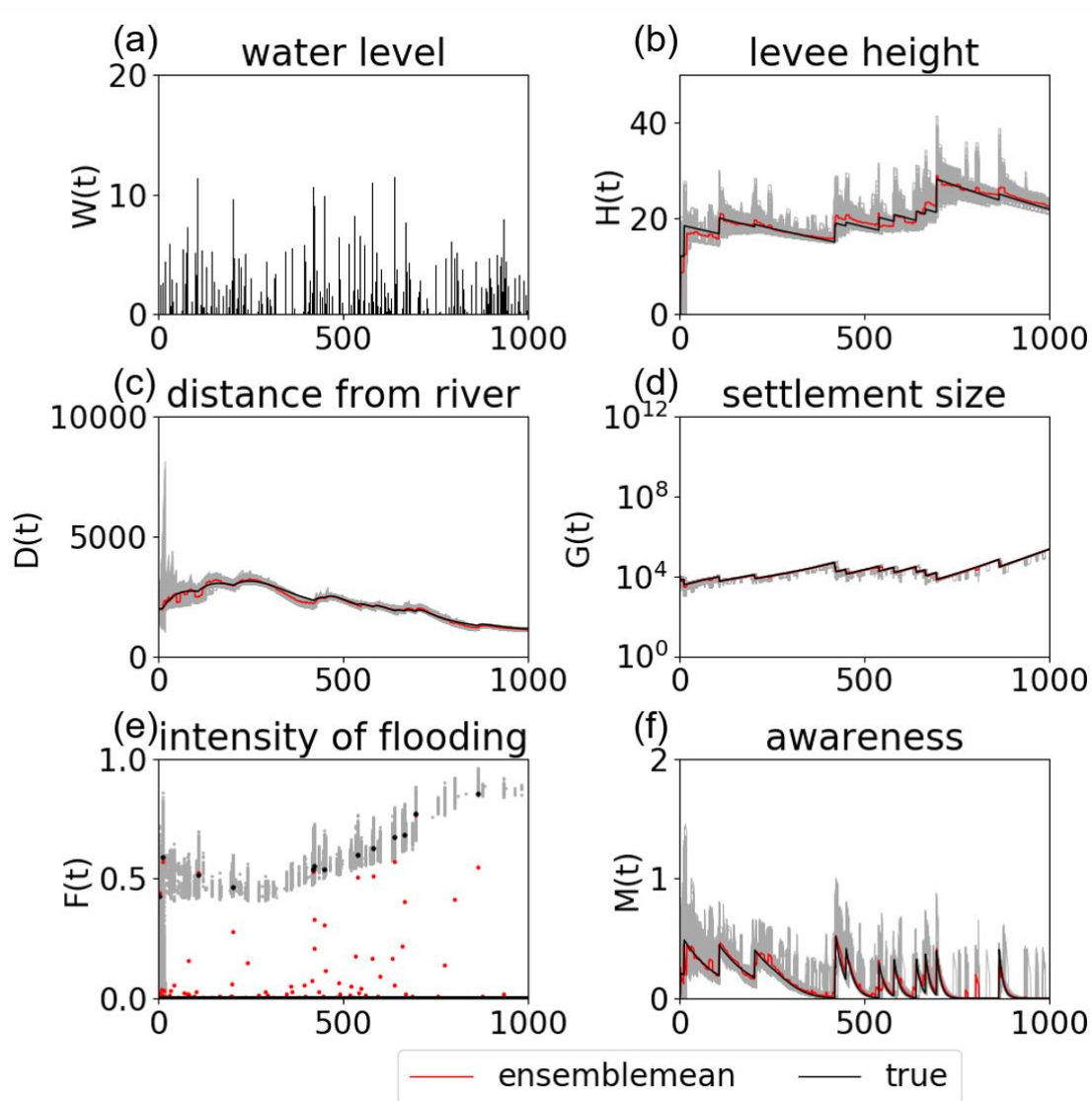
664 in the experiment 2 (see section 3.2). (a) Blue, orange, gray, and yellow bars are RMSEs of the size of the



665 human settlement $G(t)$, the center of mass of the human settlement from the river $D(t)$, the flood protection
666 level (or levee height) $H(t)$, and the social awareness of the flood risk $M(t)$. (b) Blue, orange, gray, and yellow
667 bars are RMSEs of the cost of levee raising γ_E , the rate by which new properties can be built φ_P , the rate of
668 decay of levees κ_T , memory loss rate μ_S .

669

670

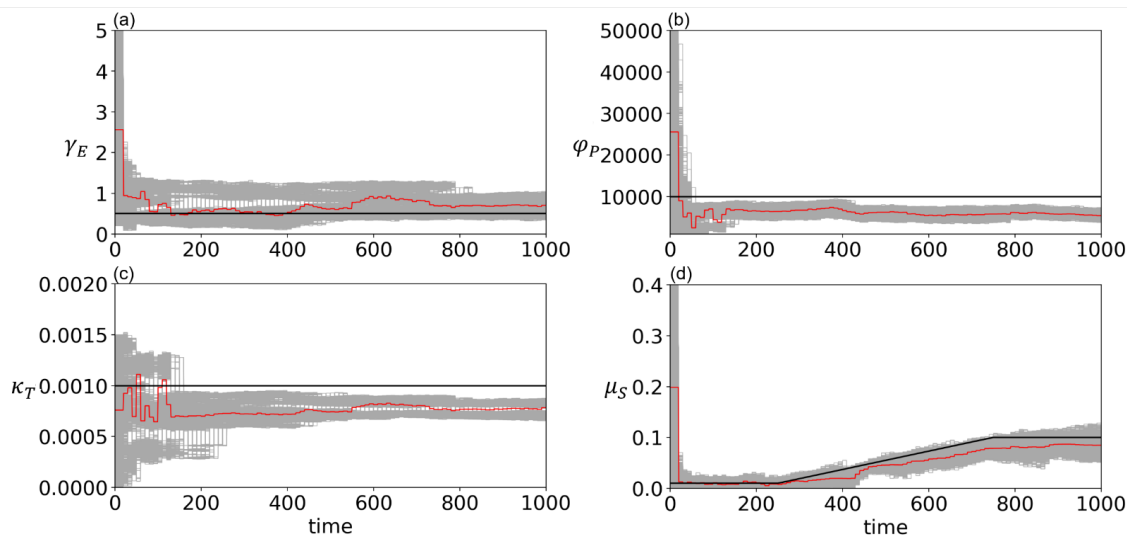


671

672 **Figure 10.** Timeseries of (a) high water level $W(t)$, (b) the flood protection level (or levee height) $H(t)$, (c) the
673 distance of the center of mass of the human settlement from the river $D(t)$, (d) the size of the human settlement
674 $G(t)$, (e) the intensity of flooding events $F(t)$, and (f) the social awareness of the flood risk $M(t)$ simulated by
675 the data assimilation experiment in which the observations of F , G , D , H , and M are assimilated into the model



676 every 10 years with 5000 ensembles in the experiment 3 (see section 3.3). Grey, red, and black lines are the
677 ensemble members, their mean, and the synthetic truth, respectively.



678

679 **Figure 11.** Timeseries of (a) the cost of levee raising γ_E , (b) the rate by which new properties can be built

680 φ_P , (c) the rate of decay of levees κ_T , (d) memory loss rate μ_S estimated by the data assimilation of all

681 observations (F, G, D, H, and M) with 5000 ensembles every 10 years in the experiment 3 (see section 3.3).

682 Grey, red, and black lines are the ensemble members, their mean, and the synthetic truth, respectively.

683

684